HHS Public Access

Author manuscript

Adv Healthc Mater. Author manuscript; available in PMC 2023 October 01.

Published in final edited form as:

Adv Healthc Mater. 2022 October ; 11(19): e2200773. doi:10.1002/adhm.202200773.

Electrochemical Sensors based on MoS_x-functionalized Laser Induced Graphene for Real-time Monitoring of Phenazines produced by *Pseudomonas aeruginosa*

Keren Zhou[1,2], **Vinay Kammarchedu**[1,2], **Derrick Butler**[1,2], **Pouya Soltan Khamsi**[1,2], **Aida Ebrahimi**[1,2,3,*]

[1]School of Electrical Engineering and Computer Science, The Pennsylvania State University, University Park, PA 16802, USA

[2]Materials Research Institute, The Pennsylvania State University, University Park, PA 16802, USA

[3]Department of Biomedical Engineering, The Pennsylvania State University, University Park, PA 16802, USA

Abstract

Pseudomonas aeruginosa (*P. aeruginosa*) is an opportunistic pathogen causing a series of infections in blood and implanted devices. Traditional identification of *P. aeruginosa* involves plating and counting colonies which takes more than 24 hours to produce results. Molecular biology methods can expedite detection, but they require advanced skill set. To address these challenges, in this work, we investigate functionalization of laser-induced graphene (LIG) to develop flexible electrochemical sensors for detecting *P. aeruginosa* based on its phenazine metabolites as biomarkers. An electrodeposition method is used as a facile and scalable approach to functionalize LIG with molybdenum polysulfide (MoS_x). The effect of electrodeposition time is studied to enhance the sensitivity. The sensor performance, including the limit of detection (LOD), sensitivity, dynamic concentration range, and specificity are determined in broth, agar, and wound simulating medium (WSM). Control experiments with *Escherichia coli* (*E. coli* which does not produce phenazines) demonstrate specificity of sensors to probe *P. aeruginosa*. The LOD of MoS_x/LIG for detecting pyocyanin (PYO) and phenazine-1-carboxylic acid (PCA) is 0.19 μM and 1.2 μM in broth, respectively. Furthermore, the sensors are highly stable and enable real-time monitoring of *P. aeruginosa* biofilms over several days with minimal degradation. Comparing different square wave voltammetry (SWV) peak currents over time shows time-dependent generation of phenazines by *P. aeruginosa* biofilm. In particular, two configurations – "Normal" and "Flipped" – are studied, showing that the phenazines time dynamics vary depending on how cells interact with sensors. The reported results demonstrate the potential of the developed flexible sensor for integration with implantable devices and wound dressings for early diagnosis of *P. aeruginosa* infection at the point of care.

*Correspondence: sue66@psu.edu.

Supporting Information

Supporting Information is available from the Wiley Online Library or from the author.

The authors have no conflict of interest.

Graphical Abstract

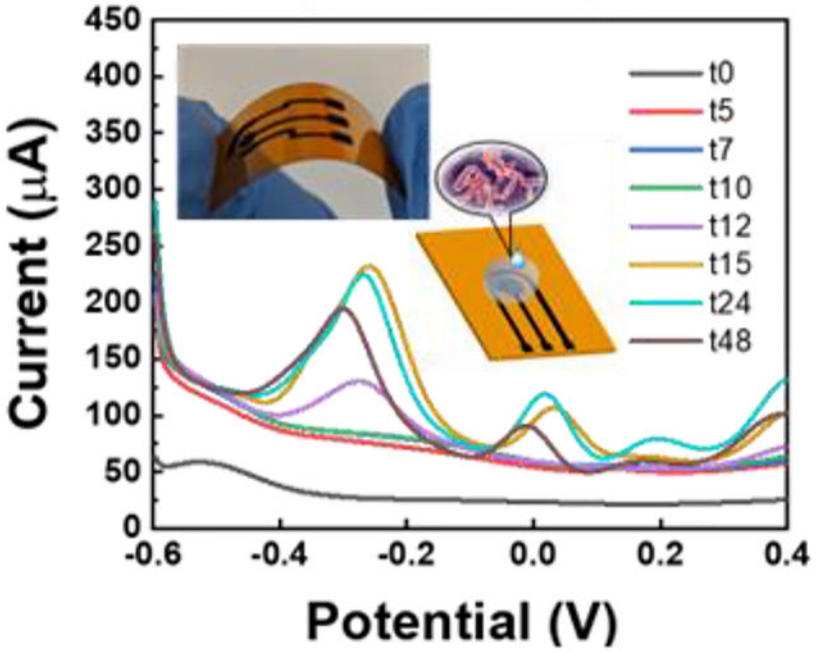

In this work, flexible electrochemical sensors based on MoS_x- functionalized laser-induced graphene are developed for monitoring phenazines produced by the opportunistic pathogen, *P. aeruginosa*. The fabrication process is simple and scalable, and the sensors enable real-time monitoring of growth of *P. aeruginosa* colony biofilms over several days.

Keywords

phenazines; electrochemical sensor; pseudomonas aeruginosa; laser induced graphene; biofilm infection; wound infection

1. Introduction

Pseudomonas aeruginosa (*P. aeruginosa*) is the pathogenic cause of a series of blood and lung infections (for example in ventilator associated pneumonia and cystic fibrosis).[1] As a common pathogen found in healthcare settings, it can also infect burns and surgical wounds. In addition, most of *P. aeruginosa* in the environment has developed antibiotic resistance, thus making routine antibiotic treatments ineffective and causing a high mortality rate in some cases.[2] To better understand its infection mechanism, monitoring growth of *P. aeruginosa* and production of specific biomarkers is necessary.[3] In particular, it has been shown that production of phenazine molecules – including pyocyanin (PYO), phenazine-1-carboxylic acid (PCA), phenazine-1-carboxamide (PCN), and a less stable intermediate 5-methylphenazine-1-carboxylic acid (5-MCA) – plays an important role during *P. aeruginosa* infections.[3] PYO, a bluish redox-active organic compound produced by *P. aeruginosa*, can induce neutrophil apoptosis (programmed cell death), cause oxidative stress to cells, and prevent the beating of lung cilia, all of which aid survival of the *P. aeruginosa* infection.

[4,5] Moreover, PYO functions as a signaling molecule in *P. aeruginosa* quorum sensing (QS). QS is a mechanism through which bacteria can monitor their population through secretion and sensing certain signaling molecules, and hence is critical in communication and decision-making in biofilms.[6] As a result, specific genes will be expressed and bacterial characteristics, such as respiration, antibiotic resistance, and virulence change.[7] These findings suggest that identifying phenazines could help us better comprehend the *P. aeruginosa* infection mechanism.

Since their discovery, phenazines have been explored using various methods. Phenazines are extracted from *P. aeruginosa* cultures by chloroform extraction techniques from supernatants of the culture or clinical samples.[8] The phenazine level is then quantified using high-performance liquid chromatography (HPLC)[9] or spectrophotometry[10] which yield micromolar limit of detection (LOD). Other analytical methods, including proton nuclear magnetic resonance,[11] Fourier transform infrared spectroscopy,[12] and matrix-assisted-laser-desorption-ionization time-of-flight (MALDI-TOF) mass spectrometry[13] have been also explored to identify phenazines. Although these methods provide good quantification, extensive sample preparation/treatment steps, such as separation of phenazines from other matrix components, are needed, leading to increase of the total analysis time and making real-time analysis challenging if not impossible. Furthermore, these methods often utilize bulky equipment, require highly skilled personal, and are not accessible to everyone, limiting their application for point of care needs or small laboratories. To address these challenges, various biosensors – including surface-enhanced Raman spectroscopy (SERS) and electrochemical methods – have been explored by the researchers.

Among different biosensor technologies, electrochemical devices are highly attractive for detecting and monitoring phenazines due to their redox active nature. Figure 1a shows the biosynthesis pathway of various phenazines in *P. aeruginosa* and their half-wave redox potential ($E_{1/2}$ = −70 mV, −247 mV, −323 mV and −347 mV vs. Ag/AgCl for 5-MCA, PYO, PCA, and PCN, respectively, at pH 7)[3]. Electrochemical biosensors are easy-to use, low-cost, rapid and sensitive, and portable.[14] In addition, they use relatively simple and low-cost instrumentation (potentiostats that can even be developed using Arduino kits[15]) and are compatible with CMOS technology for integration with data processing and transmission nodes for ultimate compactness.[16] The first electrochemical sensor for PYO used a mercury drop electrode as working electrode (WE), a Pt electrode as counter electrode (CE), and Ag/AgCl as reference electrode (RE) in a 15-mL quartz cell. PYO was detected by adsorptive stripping voltammetry (AdSV) with an oxidation peak at the potential of −0.17 V. The LOD was 2.0 nM in diluted Mueller–Hinton broth.[17] Due to their high sensitivity and good specificity, other established electrochemical methods have been reported to measure the generation of PYO in biofilms, e.g., cyclic voltammetry (CV), square wave voltammetry (SWV), differential pulse voltammetry (DPV), and electrochemical impedance spectroscopy (EIS).[18] In addition to various electrochemical measurement methods used for phenazine detection, different electrode materials and modifications, and innovative device engineering have been developed to further enhance the detection sensitivity and sensor screening capabilities. For example, Bellin et al. developed an integrated circuit (IC)-based electrochemical sensors with array of gold working electrodes for real-time monitoring of phenazine derivatives across a matured *P. aeruginosa* biofilm on agar

with high spatiotemporal resolution.[3,19] Simoska et al. used low-cost transparent carbon ultramicroelectrode arrays fabricated using polystyrene spheres. The sensors were used for in vitro detection of phenazines and studying the environmental effects on phenazine production.[20–22] Using photolithography and wet etching, Do et al. developed metal–insulator–metal ring electrode structures based on gold electrodes to improve LOD down to 10.5 nM and 20.7 nM for PYO and PCN using redox cycling amplification[23]. In another work, carbon nanotube-based sensors were prepared using inkjet printing to monitor PYO and uric acid in a wound simulating fluid.[24] And Cernat et al. prepared a Au/Ag nanoalloy in hydrogel and drop casted it on carbon electrode to detect PYO with a LOD of 40 nM.[25]. As it can be seen from this brief overview, there are various methods that have been explored for manufacturing electrochemical sensors for detecting phenazines, from ink-jet printing and drop casting to photolithography methods.[24–28] The most commonly used strategies for buidling electrochemical sensors include drop casting of the sensing material (e.g. gold nanoparticles, carbon nanotubes, nanowires) over a supporting electrode (usually carbon) [25], inkjet printing,[24] and screen printing;[29] however, these methods can leave residues on the substrate after solvent evaporation[14] and surface modification may be inhomogeneous because of the coffee ring effect[30]. In comparison, microfabrication using lithography methods offer better spatial resolution and control over the electrode geometry. However, microfabrication requires cleanroom which is not as accessible and involve multiple steps of deposition, patterning, and etching to create desired devices.[20]

To achive facile fabrication for rapid sensor prototyping, while avoding the issues with solution-based processing, we developed three dimensional (3D) graphene electrodes by direct laser writing followed by selective funcionallization using electrodeposition. Creation of laser-induced graphene (LIG) made from commercial polyimide (PI) films was first reported by Tour et al. in 2014 based on a photothermal process using CO_2 laser.[31] Owing to its unique features, including 3D microporous structure, high electrical conductivity, chemical-free, and direct patterning advantage, LIG has gained an exponentially growing interest in various fields, including biochemical sensing.[14] Furthermore, the approach is suitable for mass production of low-cost and portable sensors. Combination of these properties make LIG an ideal base material for manufacturing electrochemical biosensors. [32]

In this study, for the first time to the best of our knowledge, we report developing a LIG-based sensor for detection and monitoring phenazines produced by *P. aeruginosa* (both in biofilm studies as well as in vitro analysis in a wound simulating medium, WSM). In particular, we have studied the effect of electrochemical functionalization of LIG – as working electrode – by two materials: platinum (Pt; which is commonly used as the tip in scanning electrochemical microscopy (SECM) mapping of phenazines)[33–35] and molybdenum polysulfide (MoS_x). We show that the sensor LOD and sensitivity are improved significantly with MoS_x/LIG compared to Pt/LIG. The effect of the frequency of the square wave voltammetry (SWV) on sensor sensitivity and LOD is investigated to identify an optimum working frequency of 15 Hz in this work. The sensor response is first evaluated with synthetic PYO and PCA in brain heart infusion (BHI), as well as with cetrimide agar. Then the sensor performance for monitoring *P. aeruginosa* colony biofilms is studied on agar. Excellent long term stability of the sensors enable real time monitoring of

biofilms to characterize the dynamic nature and interplay between different phenazines over time by comparing the SWV peak currents at different potentials. Finally, we also studied phenazines and *P. aeruginosa* in a wound simulating medium to demonstrate the potential of the developed low-cost sensor for clinical settings, for example for analysis of wounds and sputum samples.

2. Results and discussion:

2.1. Fabrication, functionalization, and material characterization of electrodes

Using direct laser writing, LIG electrodes are developed as the base electrode material to replace the traditional carbon electrodes (glassy carbon electrode or screen-printed carbon). During the laser writing process, the high temperature/pressure treatment produces gas and the release of the gas forms a 3D porous structure, which has been proven to lead to higher charge transfer and improved mass transport.[36] The fabrication process of LIG and studying the effect of various conditions (substrate, writing parametrs, environment) have been extensively explored by other researchers.[37] Figure 1b shows the fabrication process and functionalization of LIG using polyimide (Kapton®, 500 HN) as the substrate and utilizing a commercial laser cutting machine (Universal Laser Systems) to create the LIG electrodes (details in Methods Section). The laser beam is focused on the substrate and controlled to carbonize polyimide in the ambient air. Then the LIG pattern is created in a desired three-electrode design. To have a better balance between the electrical conductivity and mechanical strength of the sensor, we tried different combinations of the processing parameter. The final optimized parameters are power: 6.3%, speed: 5.5%, and PPI: 1000 using Rastor mode. A thin Nafion film is spin-coated onto the electrode surface to protect the electrode from biofouling.[38] The inset shows the sensor bending, demonstrating the device's potential for flexible electronics and wearable devices, for example for integration with strain sensors,[39] ECG patches,[40] or vital-sign monitoring sensors.[41] A picture of the sensor attached to a testing connector and ready for testing is shown. Two sets of measurements are performed: in liquid (by testing is broth culture as well as wound simulating medium (WSM)) and with agar slabs to study colony biofilms. Agar is a soft material (a gel) and can mimic the tissue structure and has been used in developing in vitro wound models.[42] The tests with agar slabs are prformed in a custum-made humidity/temperature-controlled incubator (Figure S1 in Supplementray Information, SI).

Noble metals (e.g., gold, platinum)[27,43] and various two-dimensional materials (e.g., graphene, MXenes)[44,45] have been widely investigated to modify working electrode of electrochemical sensors in order to improve the sensitivity and LOD. We explore two routes for functionalizing LIG using the electrodeposition method which is a facile and scalable manufacturing process.[46] LIG is modified with Pt and MoS_x and their response to phenazines is compared which are discussed in the next section. To characterize the electrode surface morphology and chemical components, the scanning electron microscopy (SEM), X-Ray diffraction (XRD), Raman spectroscopy, and X-ray photoelectron spectroscopy (XPS) are performed. The SEM image in Figure 2a confirms a fibrous foam structure of the LIG electrode. Compared to traditional planar carbon or gold electrodes, the porous morphology of LIG leads to higher density of active and edge

sites which are found beneficial for electrodeposition, and hence improve sensor sensitivity.[14,32,39,43] Figure S2a summarizes the XRD results. The XRD of LIG shows the (002) and (100) plane of the graphite-2H (PDF 41-1487), consistant with previous reports.[31] Pt/LIG also shows the (111), (200), and (220) planes of Pt (PDF 04-0802) in addition to the graphite peaks. There's no obvious MoS_x characteristic peak found in the XRD results of the MoS_x/LIG sample since the material is amorphous.[47] The Raman spectra of LIG and MoS_x/LIG were also measured, however, as expected both were similar in most aspects and no distinct prominent peaks could be observed (Figure S2b). Due to non-planar structure of LIG most of the light is scattered and the signal obtained signal is low and does not show any detectable peaks for MoS_2 at 405 cm^{-1} and 380 cm^{-1} as reported previously.[48] Some studies report that the peak may be very weak and broad when amorphous, however is enhanced when the material is transformed to a crystalline structure, e.g. using thermal annealing.[49,50] To further study the chemical composition of MoS_x/LIG, XPS is performed and the results are plotted in Figure 2b. The survey spectrum suggests that carbon and oxygen are the main components. The high-resolution spectra of Mo 3d and S 2p orbitals are shown in Figure S2c–d. The results show that MoS_2, MoS_4, and MoO_3 are present in the sample.[51] The peaks located at ~150 eV and 100 eV are referred to the 2s and 2p peak of silicon (Si) because of silicone was used to passivate the electrode area. Figure 2c–d show mapping of S and Mo conducted by energy dispersive X-ray spectroscopy (EDS) with SEM, confiming the presence of molybdenium polysulfide on LIG, which is consistent with the XPS results.

2.2. Electrochemical measurement with synthetic phenazines and comparison of different functional layers

The effect of the SWV frequency on the sensor response is investigated first with 0.1 mM of PYO in BHI. Multiple frequencies (5–100 Hz) are explored as shown in Figure 3a (for Pt/LIG sample with 15 min deposition), showing that 15 Hz is the optimum frequency for phenazine sensing in our system. Similar frequency values was previously reported.[4,20] The current/frequency relationship in SWV reflect the rate of the electrons transfers, thus the frequcney can be tuned to distinguish reactions with different transfer rates.[52] A distinct oxidation peak is found at −0.227 V with PYO, with the peak magnitude proportional to PYO concentration after subtracting the baseline (Figure 3b). Figure 3c shows the location of PCA peak to be around −0.295 V. The relative peak location difference of PYO and PCA is measured to be ~68 mV, which is consistent with previous reports using other sensors.[3,53]

To investigate the effect of functionalization of LIG for detection of phenazines, we study three different working electrode materials: LIG, Pt/LIG, and MoS_x/LIG with PYO and PCA concentrations ranging from 0.1 to 100 uM in BHI using SWV. In particular, for each modification, we evaluate the effect of electrodeposition time in creating Pt/LIG and MoS_x/LIG. Pt is electrodepisted for 5 min, 10 min, and 15 min on LIG (Figure S3a–b), showing that the deposition time does not have a significant impact on sensor LOD and sensitivity. LOD is calculated by the concentration current 3.3 times the standard deviation of the blank solution, σ_B. The data are then fitted with a line and the slope of he linear region is considered as the sensor sensitivity. Interstingly, Pt/LIG demonstrates a LOD of

1.2 μM and 5.2 μM for PYO and PCA, respectively, which are 5 and 20 times lower than convectional Pt disk electrode. Two MoS_x deposition times are explored (30 min and 60 min). Figures 4a and 4b compare the calibration curves with PYO and PCA for MoS_x/LIG and Pt/LIG (15 min deposited samples). From these curves, LOD and sensitivity with PYO for MoS_x/LIG:30 min vs. MoS_x/LIG:60 min are respectively 0.22 μM and 0.82 μA/μM vs. 0.19 μM and 0.97 μA/μM, demonstrating that 60 min deposition offers a slightly lower LOD and higher sensitivity compared to 30 min deposition. To better understand the reaction mechanism on the modfied LIG electrode, we used the CV method with scan rates ranging from 0.01 Vs^{-1} to 0.2 Vs^{-1}. The linear fitting and corresponding electrochemically active surface area (ECSA) are obtained from the relation between the CV current peak and the square root of the scan rate, as shown in Figure S4. The coefficient of determination (R^2) of the linear fitting for LIG, Pt/LIG and MoS_x/LIG is 99%, 97% and 98%, respectively. The results suggest that PYO oxidation on all materials is a diffusion-limited process, following the Randles-Sevcik equation.

$$i_{peak} = 0.4463n^{1.5}F^{1.5}CA\sqrt{\frac{Dv}{RT}}, \quad \text{Eq. 1}$$

Where i_{peak} is the peak current (oxidation), n is the number of transferred electrons (here $n = 2$), F is the faraday's constant, D is the diffusion coefficient of PYO (here $D = 7.2 \times 10^{-6} cm^2 s^{-1}$), C is the concentration of PYO (here $C = 10^{-4}$ M), A is ECSA, R is the universal gas constant, T is the temperature, and v is the cyclic voltammetry scan rate. The calculated ECSA for LIG, Pt/LIG and MoSx/LIG is 2.26, 4.06 and 5.39 mm^2, respectively. MoSx/LIG shows the largest ECSA, contributing to its improved sensitivity to phenazines.

In addition, MoSx/LIG samples (both 30 min and 60 min deposition) are more sensitive for detecting PYO than Pt/LIG (with LOD of 1.2 μM). The LOD of PCA with MoS_x/LIG (1.2 μM) and Pt/LIG (5.2 μM) are also calculated from the calibration curves in Figure 4b, further confirming the superior response of MoS_x/LIG compared to Pt/LIG. Additional benefits of MoS_x/LIG over Pt/LIG include lower reagent cost and a gentle and environmental friendly deposition solution; MoS_x deposition is done in KCl solution at neutral pH while Pt is achieved in an acidic environment. Interestingly, with deposition of MoS_x on LIG, antibacterial effects on cell suspensions are reduced in time-dependent studies (Figure S5a). That said, without Nafion, cell count with MoS_x/LIG sample is 70% lower than the control sample (Kapton film) and almost the same with LIG. The results we obtained with LIG are consistent with previous reports.[54,55] With increasing incubation time (from 2hr to 4 hr), cell viability decreases. By coating the electrodes with Nafion (Figure S5b), the antibacterial properties of both LIG and MoS_x/LIG reduces. Specifically, Nafion seems to affect MoS_x/LIG more prominently (viability after 4 hrs is significantly higher with Nafion compared to without Nafion in Figure S5a. We also observe increased hydrophobicity of the electrodes surface after coating the Nafion (Figure S6) which may explain reduced interaction with cells and hence improved viability.[56]

It should be noted that our results show that LOD of Pt/LIG is comparable with bare LIG. In addition, the performance of the standard Pt disk is worse than all developed sensors,

indicating that Pt may not be the best electrode material for sensing phenazines despite being extensively used for detecting phenazine, e.g. in scanning electrochemical microscopy (SECM) analyses.[57,58] Our results are consistent with previous studies which demonstrated that carbon constitutes a more suitable material for PYO detection, because of the overlap of the benzene ring in PYO and the carbon molecular structure.[59] The previous reports based on electrochemical detection of PYO are summarized in Table 1. Majority of the works used gold or carbon as the WE material. Compared to gold, carbon is a more affordable choice for constructing low cost sensors. However, the prior reported works are mostly based on drop-casting, screen printing, or inkjet printing of the carbon-based materials (carbon paste/ink, carbon nanotubes/fibers). As noted before, in contrast to our work which is based on direct laser processing of plastic and electrodeposition (both scalable and facile processes), these deposition/printing methods suffer from poor adhesion between the sensing layer and the supporting substrate. We also study the effect of storage condition (as-prepared, 3 days storage in ambient air, and 3 days storage in a N_2 desiccator) with PYO and PCA, confirming excellent stability of LIG in ambient environment (Figure S3c–d). Given the superior performance of MoS_x/LIG, this material is chosen for studies with bacteria.

2.3. In vitro colony biofilm studies: Impact of sensor-cell intercation and cell seeding density

In this section, we investigate two configuartions with colony biofilms on agar (as nutrition source and in vitro model for tissue): (1) “Normal” test (inset of Figure 5a), where agar separates cells from the sensor and (2) “Flipped” test (Figure 6a), where cells are overlaid by the agar and are in direct contact with the sensor. These studies allow us to mimic surface vs. deep tissue infections with agar acting as a tissue model.

In “Normal” test, agar works as a protective layer as well.[19] In this case, it takes more time for phenazine molecules to diffuse from the top of the agar to the electrode surface. Hence, before experiments with cells, we first determine the diffusion constant of PYO and PCA in agar. We perform SWV measurements over time after placing a thin agar slab on the sensor and adding a droplet of the BHI broth spiked with PYO or PCA. The raw SWV plots with 5 μL of 1 mM PYO, 0.5 mM PYO, and 0.2 mM PYO are shown in Figure S7. We calculate the diffusion coefficient (D) of PYO and PCA based on fitting the data in Figure 4c using Fick’s second law of diffusion ($\frac{\partial C}{\partial t} = D\nabla^2 C$) and assuming that concentration of the molecules is proportional to the peak current. The calculated D_{PYO} and D_{PCA} are 6×10^{-10} m^2/s and 2×10^{-10} m^2/s, which are close to the values reported elsewhere.[3]

After the diffusion tests, we move to experiments with cells. We inoculate cetrimide agar (thickness of t= 2 mm, diameter of d= 6 mm) with 5 μL suspnesions of *E. coli* (as negative control; Figure 5a) or *P. aeruginosa* (PA14; Figure 5b) each diluted at 1:100 from the overnight culture which yields 2.8×10^7 CFU/mL. The number of seeded cells is estimated to be 1.4×10^5 CFU with 1:100 dilution. Figure 5a and b show the SWV measurement with “Normal” configuration with negative control and PA14 strain collected over time. The peak of PYO (~ −0.25 V) is detectable starting at 12 hours after inoculation. The peak then grows up within 24 hours and then goes down at 48 hours. We also explore the effect of the inoculation/seeding density by changing the dilution factor from 1:100 to 1:10 (i.e.

approximately 1.4×10^6 CFU added on agar). Figure 5c shows the SWV results over time, indicating that peak of PYO can be observed at 7 hours after inoculation. To show the results more clearly, we plot the peak current at −0.25 V over time in Figure 5d. The increase in the initial cell denisty is expected to allow faster detection of phenazines than the more dilute solution due to larger amount of biomass.

Schemtic of the "Flipped" test is shown in Figure 6a, where *P. aeruginosa* culture is first dropped on the agar top, then the agar is flipped. Figure 6b shows the SWV results of the MoS_x/LIG sensor with this configuration with 5 μL of 1:100 diluted PA14. By comparing the peak current values for "Normal" vs. "Flipped" configuration in Figure 6c, it is seen that the latter leads to faster detection of phenazines, which is expected since cells are closer to the sensor. Our results also demonstrate that there is a dynamic behavior in production of different phenazines by cells. For example, two largest peaks (Peak 1: PYO and PCA, Peak 2: 5-MCA) are highlighted with arrows in Figures 5b and 6b. By plotting the time-evolution of the average ratio of Peak 2/Peak 1 in Figure 6d, we observe that this ratio increases over time, indicating that the production rate of different phenazines is dynamic and evolves with time, consistent with previous reports.[22] These results demonstrate the sensor's success in monitoring the dynamic nature and interplay between different phenazines over time. Before concluding this section, it should be noted that depending on *P. aeruginosa* strain, different rates and dynamics of phenazine production can be observed, as can be seen from Figure S8a using PA strain ATCC 9027. This strain with defectivce mutant is unable to produce PYO in LB, which has been reported elsewhere.[60] In addition to strain, the medium can also impact phenazine production. For example, we observe different phenazine time profiles when cells are on LB agar (see Figure S8b) compared to cetrimide agar, which is consistant with previous reports.[61]

In addition to colony biofilm studies on agar, we demonstrate that MoS_x/LIG sensors can successfully detect and monitor phenaiznes produced by *P. aeruginosa* in a wound simulating medium (WSM). Figure 7a shows the SWV curves with 0.1~100 uM PYO spiked in WSM. Figure 7b plots the calibration curve with PYO obtained from six independent sensors. Compared to tests in BHI, the LOD of the sensor gets higher, but it is still about 1.3 μM. This LOD is sufficient for detecting and monitoring phenazines in *P. aeruginosa*. For example, in sputum sample, PYO is found to be up to 130 μM.[4] The sensor response is monitored over 24 hours with PA14 cultures in WSM (Figure 7c), showing that the PYO peak can be detected within 10 hours. The results presented in this work demonstrate the potential of the developed MoS_x/LIG sensors as a low-cost diagnostic device which can be integrated with other printable sensors (also based on LIG) for monitoring of other signals of infection, including tempearture,[41] pH,[46] blood oxygen,[62] skin impedance,[63] among others, which may enable smart therapeutics by combining early diagnosis with treatments.

3. Conclusion

In this study, a LIG-based flexible electrochemical sensor is developed and used for selective identification of multiple phenazines in bacterial culture medium, wound simulating medium, and in real-time studies with *P. aeruginosa* colony biofilms on agar. Square wave voltammetry (SWV) is utilized to monitor the sensor response over time. To further

optimize the sensor performance, the effect of LIG functionalization and SWV frequency are investigated. The LOD of the MoS_x/LIG with PYO and PCA in broth is 0.19 μM and 1.2 μM, respectively, an improvement of 6.3 and 4.3 times compared to Pt/LIG and LIG electrodes. We specifically investigate the sensor performance for real time monitoring of *P. aeruginosa* biofilm on agar through two complementary test confiurations mimicing surface vs. deep tissue infections. The production of multiple phenazines can be detected within 12 hours after 5,000 CFU/mm^2 seeding. The detection time reduces to 7 hours with 10 times higher cell density. By comparing the SWV peaks at different potential values over time, the sensor can also highlight the dynamic nature and interplay between different phenazines in *P. aeruginosa* biofilm. The sensor has the potential to be used in medical care settings, especially for detection of *P. aeruginosa* infection in wound, sputum, or on medical devices. The sensors are highly stable and enable monitoring biofilms over several days with negligible degradation.

4. Materials and Methods

4.1 Materials

Polyimide (PI) sheets are purchased from DuPont de Nemours, Inc. (Kapton® HN, 500 mils). Brain-Heart Infusion powder, Cetrimide agar, Lennox L agar, ammonium tetrathiomolybdate (CAS: 15060-55-6), pyocyanin (CAS: 85–66-5), potassium hexachloroplatinate (CAS: 16921-30-5), sodium bisulfite (CAS: 7631-90-5), and sodium thiosulfate (CAS: 7772-98-7) are purchased from Sigma Aldrich. Phenazine-1-carboxylic acid (CAS: 2538-68-3) is purchased from Apollo Scientific. Dragon Skin™ silicone rubber is purchased from SmoothOn, Inc. The platinum disk counter electrode (CE, Bioanalytical Systems #MW-4130), Ag/AgCl reference electrode (RE, Bioanalytical Systems, #MF-2052), and PalmSens4 potentiostat used in electrochemical experiments are purchased from BASi Inc.

4.2 LIG fabrication and electrochemical functionalization

The PI sheets are cropped and affixed to a glass side using a double-sided tape for easy handling during printing and functionallization. Then the LIG pattern is created using the Universal Laser Systems purchased from (VSL2.30 Desktop, 25 W) with an optimized parameter (Power 10.5%, speed 5.5%, points per inch 1,000), with the design drawn in AutoCAD®. After printing the base LIG electrodes (for working electrode: WE, counter electrode: CE, and reference electrode: RE), the sensor region are separated from the contact pads using Dragon Skin silicone rubber to prevent liquid diffusion towards the contact pads. Then the WE and RE are created using the electrodeposition method individually. We explored platinum (Pt) and MoS_x as the WE material. Pt nanocrystals are deposited on WE under a constant potential of 0.05V vs. Ag/AgCl for 600 sec using a 0.5 M sulfuric acid solution containing 2 mM Potassium hexachloroplatinate. The MoS_x nanocrystals are deposited on WE via the previously reported method.[64] Briefly, the solution contains 1 mg/ml $(NH_4)_2MoS_4$ and KCl and the WE is biased at – 0.8 V for 30 mins. Silver (Ag) is deposited on the RE with a constant current density of −150 μA/mm^2 for 300 sec using a solution containing 250 mM silver nitrate, 750 mM sodium thiosulfate, and 500 mM sodium bisulfite. Afterward, the device is washed gently in Ultrapure MilliQ deionized (DI) water

three times and dried in the fume hood. Finally, 2% Nafion in ethanol iis spin-coated onto the sensor at a spin rate of 3000 rpm for 30 seconds.

4.3 Characterization of the functionalized LIG electrodes

XRD was performed using a Malvern Panalytical Empyrean diffractometer fitted with a copper (Kα1–2 = 1.540598/1.544426 Å) long-fine-focus X-ray tube operated at 45 kV and 40 mA. The sample were front-loaded into a silicon zero background holder and diffraction data were collected from 10° to 70 °. Raman spectroscopy was carried out using a Horiba LabRam instrument (Kyoto, Japan) with a 100x objective and 1800 g/mm grating. A 532-nm wavelength laser operating at 25% of 110mW was used. Scanning electron microscopy (SEM) micrographs are taken using a ThermoFisher Verios instrument. The samples are sputter coated with ~ 5 nm of iridium prior to imaging to minimize charging. Energy dispersive X-ray spectroscopy (EDS) measurements are taken using a 10 kV beam to ensure all relevant elements are detected. X-ray photoelectron spectroscopy (XPS) measurements are performed using a Physical Electronics VersaProbe II instrument with an Al Kα X-ray source (1.49 keV). Charge calibration is done using the sp2 carbon peak at 284.4 eV. Spectra are processed and analyzed with the CasaXPS software, and the program's instrumental relative sensitivity factors are used to calculate atomic percentages.

4.4 Electrochemical tests and sensor calibration with synthetic phenazines

For creating the calibration curves, stock solutions (2 mM PYO and 500 μM PCA) are first prepared for each phenazine in ethanol. The phenazine stock solutions are then serially diluted to 100 nM, 1 μM, 5 μM, 10 μM, 50 μM, and 100 μM in BHI and used directly for electrochemical measurements. Electrochemical data is measured using PalmSens4 (BASi Inc.) in a standard three-electrode system (Pt/LIG WE, Ag/LIG RE, and LIG CE). The sensor is attached to a Zero Insertion Force (ZIF) socket and connected to the PalmSens4 with Dupont wires. The effect of SWV frequency is studied with 0.1 mM PYO at first. Unless otherwise indicated, for testing sensors in liquid, 100 μL sample solution is deposited on the sensor and characterized using SWV with the frequency of 15 Hz from −0.6 to 0 V after 3 minutes (to reach equilibrium after depositing the solution on the sensor). Between different testing solutions, the samples are cleaned by pipetting a drop of deionized water, allowing it to sit for at least 10 seconds, then removed. Cyclic voltammetry (CV) is perfomed from −0.6 to 0.2 V with 5 mV step size and a series of scan rates to calculate the ECSA. The phenazines in BHI are also dropped on top of the agar slab (with diameter of d=6 mm and thickness of t= 2 mm) placed on the sensor to study the diffusion. The agar is first prepared in a petri dish and then cut by a sterile biopsy punch (Ted Pella ®) to obtain a uniform area.

4.5 P. aeruginosa cultures and monitoring biofilms on nutritious agar

Both *P. aeruginosa* strains are cultured from frozen stock at −80 °C with lysogeny broth (LB, Lennox). Then the culture are streaked on the LB agar to get the single colony. The overnight cultures are prepared by resuspending the single colony into LB and cultured overnight (37 °C, 210 RPM shaking). To monitor the growth of *P. aeruginosa* biofilms, cells (from overnight culture; OD_{600nm}= 2, optical density unit (OD) is equal to ~1.4×10^9 CFU ml^{-1}) are first inoculated on an agar slab placed on the LIG sensor. We studied two cases

of initial cell seeding density: 5,000 CFU/mm^2 and 50,000 CFU/mm^2 dropped over the agar slab. The cetrimide agar is used to prevent other microbes' growth. The sensors with *P. aeruginosa* on an agar slab are then moved to a 6-well plate, and placed in the custum-made incubator (37 °C, 90% humidity). The electrochemical measurements are performed using a script to control the PalmSens4 at specific time points after starting the inoculation.

4.6 Tests with P. aeruginosa in wound simulating media (WSM)

The electrochemical tests of *P. aeruginosa* in wound simulating media (WSM) are performed using SWV measurement as discussed before. The overnight culture of *P. aeruginosa* is diluted 10 times with the WSM and then incubated for testing (37 °C, 210 RPM). The WSM is prepared according to a previously reported method, with 50% LB, 25% lysed human blood (Innovative Research), and 25% bovine plasma (Sigma-Aldrich).[65] The overnight culture of PA14 strain is diluted by 10 times with WSM and cultured at 37 °C with 210 RPM shaking, then 100 μL of the culture is dropped on the sensor for SWV tests over time.

4.7 Studying antibacterial effect of MoS_x/LIG compared to LIG

The LIG samples are first prepared in a 10 × 10 mm square pattern and after depositing MoSx, the MoSx/LIG and LIG are coated with Nafion. Uncoated samples are also tested to evaluate the effect of Nafion. All samples are taped with a double-sided adhesive tape to a sterile glass slide and placed inside a 6-well plate. After sterilization using UV light, 25 μL of the 1:10 diluted overnight culture is dropped on all the samples. After 2 and 4 hours, the samples are moved to a vial containing 1 mL PBS and sonicated for 1 min to transfer cells to the solution. Then the solution is diluted and spread on LB agar plates (10 cm diameter), followed by overnight incubation at 37°C to quantify viable CFUs.

4.8 Statistical Analysis

All the raw data from SWV and CV methods are processed as follows: after subtracting the baseline, peak height is calculated using PSTrace software (Palmsens Inc.). The calibration curves and barplots in Figures 5–7 are plotted using the mean and standard error of the data from 3 individual sensors (indpendtly fabricated) and 3 scans for each sensor (n=9 in total). All the statistical analysis is done using the OriginPro software.

Supplementary Material

Refer to Web version on PubMed Central for supplementary material.

Acknowledgments

We thank Riess Graduate Fellowship awarded to K. Z. and V. K., the start-up funding to A.E. by the Pennsylvania State University, and partial support from NSF:I/UCRC Phase II: Center for Atomically Thin Multifunctional Coatings (ATOMIC; Award #2113864) and the National Institutes of Health (award numbers R21EB031354 and R21GM132793). The content of this report is solely the responsibility of the authors and does not necessarily represent the official views of the National Science Foundation (NSF) or National Institutes of Health (NIH). The PA14 strain (NR-50573) was obtained through BEI Resources, NIH: National Institute of Allergy and Infectious Diseases (NIAID). The authors thank Dr. Nichole M. Wonderling at the Materials Characterization Lab (MCL, Penn State University) for their help with the XRD measurement and analysis.

References

[1]. Khalifa MM, Elkhawaga AA, Hassan MA, Zahran AM, Fathalla AM, El-Said WA, El-Badawy O, Sci. Rep 2019, 9, 1. [PubMed: 30626917]

[2]. Costerton JW, Stewart PS, Greenberg EP, Science (80-.). 1999, 284, 1318.

[3]. Bellin DL, Sakhtah H, Rosenstein JK, Levine PM, Thimot J, Emmett K, Dietrich LEP, Shepard KL, Nat. Commun 2014, 5, 3256. [PubMed: 24510163]

[4]. Webster TA, Sismaet HJ, Conte JL, ping I Chan J, Goluch ED, Biosens. Bioelectron 2014, 60, 265. [PubMed: 24813917]

[5]. Webster TA, Goluch ED, Lab Chip 2012, 12, 5195. [PubMed: 23108351]

[6]. Passador L, Cook JM, Gambello MJ, Rust L, Iglewski BH, Science (80-.) 1993, 260, 1127.

[7]. Liu L, Cao X, Ma W, Chen L, Li S, Hu B, Xu Y, Sensors Actuators B Chem 2021, 327, 128945.

[8]. King M, Guragain M, Sarkisova S, Patrauchan M, BIO-PROTOCOL 2016, 6, DOI 10.21769/BIOPROTOC.2042.

[9]. Villageliú D, Lyte M, PLoS One 2018, 13, 1.

[10]. DeBritto S, Gajbar TD, Satapute P, Sundaram L, Lakshmikantha RY, Jogaiah S, ichi Ito S, Sci. Reports 2020 101 2020, 10, 1.

[11]. El-Fouly MZ, Sharaf AM, Shahin AAM, El-Bialy HA, Omara AMA, J. Radiat. Res. Appl. Sci 2015, 8, 36.

[12]. Heydorn A, Ersboll BK, Hentzer M, Parsek MR, Givskov M, Molin S, Microbiology 2000, 146, 2409. [PubMed: 11021917]

[13]. Croxatto A, Prod'hom G, Greub G, FEMS Microbiol. Rev 2012, 36, 380. [PubMed: 22092265]

[14]. de Araujo WR, Frasson CMR, Ameku WA, Silva JR, Angnes L, Paixão TRLC, Angew. Chemie 2017, 129, 15309.

[15]. Meloni GN, J. Chem. Educ 2016, 93, 1320.

[16]. Huang Y, Mason AJ, Lab Chip 2013, 13, 3929. [PubMed: 23939616]

[17]. Vukomanovic DV, Zoutman DE, Marks GS, Brien JF, Van Loon GW, Nakatsu K, J. Pharmacol. Toxicol. Methods 1996, 36, 97. [PubMed: 8912228]

[18]. Bukelman O, Amara N, Mashiach R, Krief P, Meijler MM, Alfonta L, Chem. Commun 2009, 2836.

[19]. Bellin DL, Sakhtah H, Zhang Y, Price-Whelan A, Dietrich LEP, Shepard KL, Nat. Commun 2016, 7, 10535.

[20]. Elliott J, Simoska O, Karasik S, Shear JB, Stevenson KJ, Anal. Chem 2017, 89, 6285. [PubMed: 28558232]

[21]. Simoska O, Sans M, Eberlin LS, Shear JB, Stevenson KJ, Biosens. Bioelectron 2019, 142, 111538.

[22]. Simoska O, Sans M, Fitzpatrick MD, Crittenden CM, Eberlin LS, Shear JB, Stevenson KJ, ACS Sensors 2019, 4, 170. [PubMed: 30525472]

[23]. Do H, Kwon SR, Baek S, Madukoma CS, Smiley MK, Dietrich LE, Shrout JD, Bohn PW, Analyst 2021, 146, 1346. [PubMed: 33393560]

[24]. Jarošová R, McClure SE, Gajda M, Jović M, Girault HH, Lesch A, Maiden M, Waters C, Swain GM, Anal. Chem 2019, 91, 8835. [PubMed: 31198034]

[25]. Cernat A, Canciu A, Tertis M, Graur F, Cristea C, Anal. Bioanal. Chem 2019 41117 2019, 411, 3829. [PubMed: 31172234]

[26]. Buzid A, Shang F, Reen FJ, Muimhneacháin E, Clarke SL, Zhou L, Luong JHT, O'Gara F, McGlacken GP, Glennon JD, Sci. Reports 2016 61 2016, 6, 1.

[27]. Elkhawaga AA, Khalifa MM, El-badawy O, Hassan MA, El-Said WA, PLoS One 2019, 14, e0216438. [PubMed: 31361746]

[28]. Alatraktchi F. A. Z. a., Dimaki M, Støvring N, Johansen HK, Molin S, Svendsen WE, Anal. Biochem 2020, 593, 113586.

[29]. Alatraktchi FA, Andersen SB, Johansen HK, Molin S, Svendsen WE, Sensors 2016, Vol. 16, Page 408 2016, 16, 408.

[30]. Kaliyaraj Selva Kumar A, Zhang Y, Li D, Compton RG, Electrochem. commun 2020, 121, 106867.

[31]. Lin J, Peng Z, Liu Y, Ruiz-Zepeda F, Ye R, Samuel ELG, Yacaman MJ, Yakobson BI, Tour JM, Nat. Commun 2014, 5, 5714. [PubMed: 25493446]

[32]. Wan Z, Nguyen NT, Gao Y, Li Q, Sustain. Mater. Technol 2020, 25, e00205.

[33]. Connell JL, Kim J, Shear JB, Bard AJ, Whiteley M, Proc. Natl. Acad. Sci. U. S. A 2014, 111, 18255.

[34]. Joshi VS, Kreth J, Koley D, Anal. Chem 2017, 89, 7709. [PubMed: 28613833]

[35]. Darch SE, Koley D, Proc. R. Soc. A Math. Phys. Eng. Sci 2018, 474, 20180405.

[36]. Qiu HJ, Guan Y, Luo P, Wang Y, Biosens. Bioelectron 2017, 89, 85. [PubMed: 26711357]

[37]. Li Y, Luong DX, Zhang J, Tarkunde YR, Kittrell C, Sargunaraj F, Ji Y, Arnusch CJ, Tour JM, Adv. Mater 2017, 29, 1700496.

[38]. Wang J, Musameh M, Lin Y, J. Am. Chem. Soc 2003, 125, 2408. [PubMed: 12603125]

[39]. Zhu J, Huang X, Song W, ACS Nano 2021, 15, 18708.

[40]. Sun B, McCay RN, Goswami S, Xu Y, Zhang C, Ling Y, Lin J, Yan Z, Sun B, Goswami S, et al., Adv. Mater 2018, 30, 1804327.

[41]. Yang Y, Song Y, Bo X, Min J, Pak OS, Zhu L, Wang M, Tu J, Kogan A, Zhang H, et al., Nat. Biotechnol 2020, 38, 217. [PubMed: 31768044]

[42]. Dusane DH, Lochab V, Jones T, Peters CW, Sindeldecker D, Das A, Roy S, Sen CK, Subramaniam VV, Wozniak DJ, et al., Sci. Reports 2019 91 2019, 9, 1.

[43]. Nayak P, Kurra N, Xia C, Alshareef HN, Adv. Electron. Mater 2016, 2, 1600185.

[44]. Peng Z, Tao LQ, Zou S, Zhu C, Wang G, Sun H, Ren TL, Chem. Eng. J 2022, 428, 131079.

[45]. Li D, Shao Y, Zhang Q, Qu M, Ping J, Fu Y, Xie J, Analyst 2021, 146, 5704. [PubMed: 34515697]

[46]. Bolotsky A, Muralidharan R, Butler D, Root K, Murray W, Liu Z, Ebrahimi A, Biosens. Bioelectron 2021, 172, 112615.

[47]. Doan-Nguyen VVT, Subrahmanyam KS, Butala MM, Gerbec JA, Islam SM, Kanipe KN, Wilson CE, Balasubramanian M, Wiaderek KM, Borkiewicz OJ, et al., Chem. Mater 2016, 28, 8357.

[48]. Li H, Zhang Q, Yap CCR, Tay BK, Edwin THT, Olivier A, Baillargeat D, Adv. Funct. Mater 2012, 22, 1385.

[49]. Jagminas A, Niaura G, Žalneravičius R, Trusovas R, Račiukaitis G, Jasulaitiene V, Sci. Reports 2016 61 2016, 6, 1.

[50]. Jagminas A, Niaura G, Žalneravičius R, Trusovas R, Račiukaitis G, Jasulaitiene V, Sci. Reports 2016 61 2016, 6, 1.

[51]. Wang HW, Skeldon P, Thompson GE, Surf. Coatings Technol 1997, 91, 200.

[52]. White RJ, Plaxco KW, Anal. Chem 2010, 82, 73. [PubMed: 20000457]

[53]. Bellin DL, Sakhtah H, Zhang Y, Price-Whelan A, Dietrich LEP, Shepard KL, Nat. Commun 2016, 7, 1.

[54]. Singh SP, Li Y, Be'Er A, Oren Y, Tour JM, Arnusch CJ, ACS Appl. Mater. Interfaces 2017, 9, 18238.

[55]. Huang L, Xu S, Wang Z, Xue K, Su J, Song Y, Chen S, Zhu C, Tang BZ, Ye R, ACS Nano 2020, 14, 12045.

[56]. Adabi M, Naghibzadeh M, Adabi M, Zarrinfard MA, Esnaashari SS, Seifalian AM, Faridi-Majidi R, Tanimowo Aiyelabegan H, Ghanbari H, 10.1080/21691401.2016.1178134 2016, 45, 833.

[57]. Carano M, Holt KB, Bard AJ, Anal. Chem 2003, 75, 5071.

[58]. Katemann BB, Schuhmann W, Electroanalysis 2002, 14, 22.

[59]. Alatraktchi FA, Svendsen WE, Molin S, Sensors (Switzerland) 2020, 20, 1.

[60]. García-Reyes S, Cocotl-Yañez M, Soto-Aceves MP, González-Valdez A, Servín-González L, Soberón-Chávez G, Mol. Microbiol 2021, 116, 1113. [PubMed: 34418194]

[61]. King EO, Ward MK, Raney DE, J. Lab. Clin. Med 1954, 44, 301. [PubMed: 13184240]

[62]. Zhang C, Chen H, Ding X, Lorestani F, Huang C, Zhang B, Zheng B, Wang J, Cheng H, Xu Y, Appl. Phys. Rev 2022, 9, 011413.

[63]. Hossain MF, Heo JS, Nelson J, Kim I, Inf 2019, Vol. 10, Page 325 2019, 10, 325.

[64]. Lei Y, Butler D, Lucking MC, Zhang F, Xia T, Fujisawa K, Granzier-Nakajima T, Cruz-Silva R, Endo M, Terrones H, et al., Sci. Adv 2020, 6, 4250.

[65]. Crone S, Garde C, Bjarnsholt T, Alhede M, 10.12968/jowc.2015.24.2.64 2015, 24, 64.

[66]. Kim E, Gordonov T, Bentley WE, Payne GF, Anal. Chem 2013, 85, 2102. [PubMed: 23311878]

[67]. Burkitt R, Sharp D, Electrochem. commun 2017, 78, 43.

[68]. Ciui B, Tertiş M, Cernat A, Săndulescu R, Wang J, Cristea C, Anal. Chem 2018, 90, 7761. [PubMed: 29851349]

[69]. Sharp D, Gladstone P, Smith RB, Forsythe S, Davis J, Bioelectrochemistry 2010, 77, 114. [PubMed: 19666245]

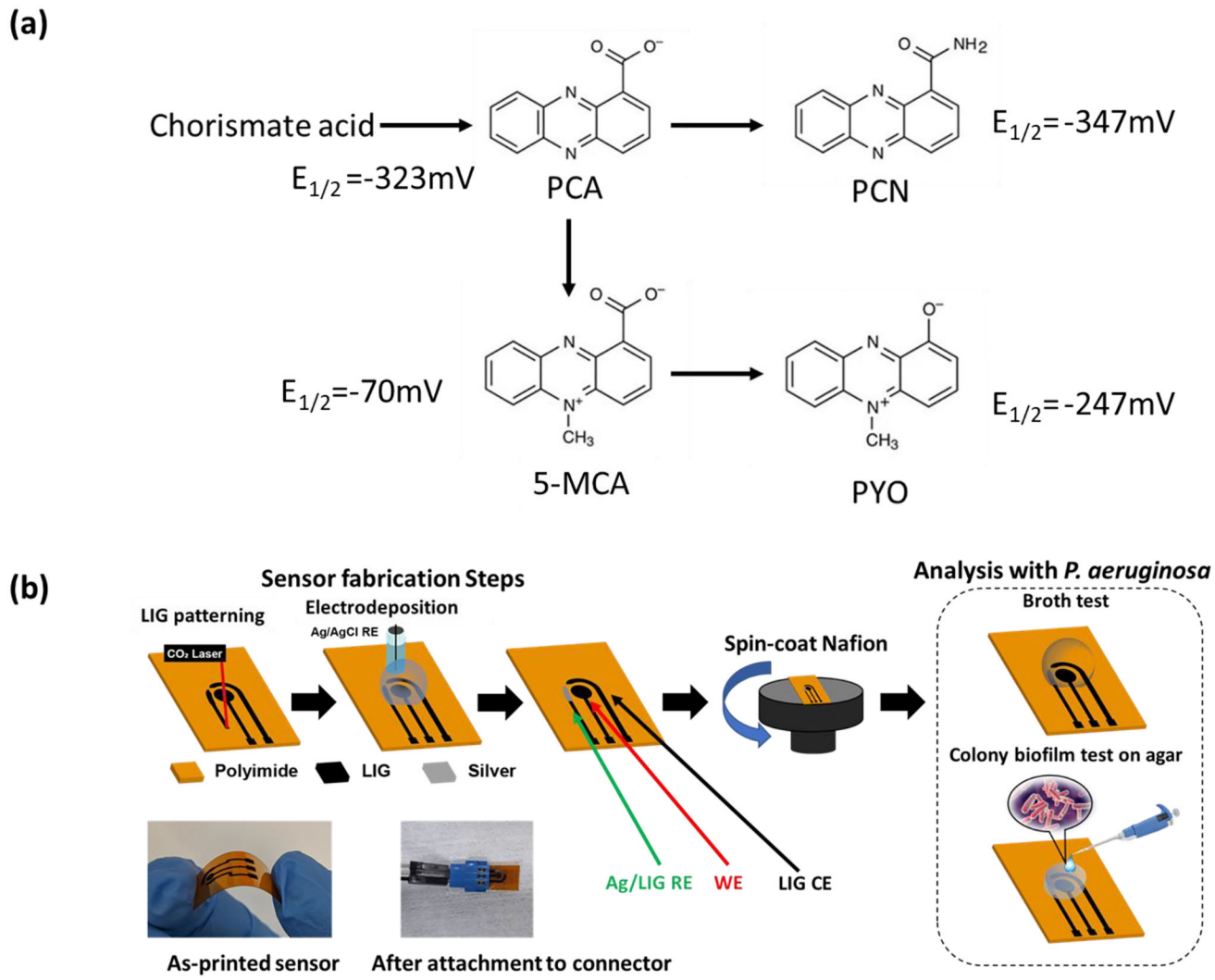

Figure 1.

(a) Synthesis pathway of phenazine metabolites with half-wave redox potentials ($E_{1/2}$) relative to Ag/AgCl at pH 7. **(b)** A schematic of the sensor fabrication and functionalization process: The 3-electrode pattern is created by laser engraving machine, then the working electrode (WE) was functionalized with Pt nanoparticles, following electrodeposition silver (Ag) on the reference electrode (RE). Finally, the sensor is spin-coated with Nafion membrane and attached to the connector for electrochemical testing. Two sets of electrochemical tests are performed using the sensors: in vitro analysis with broth and simulating medium (WSM) and long-term monitoring of colony biofilms on agar. Example pictures of the as-fabricated sensor and after attachment to the test connector are shown.

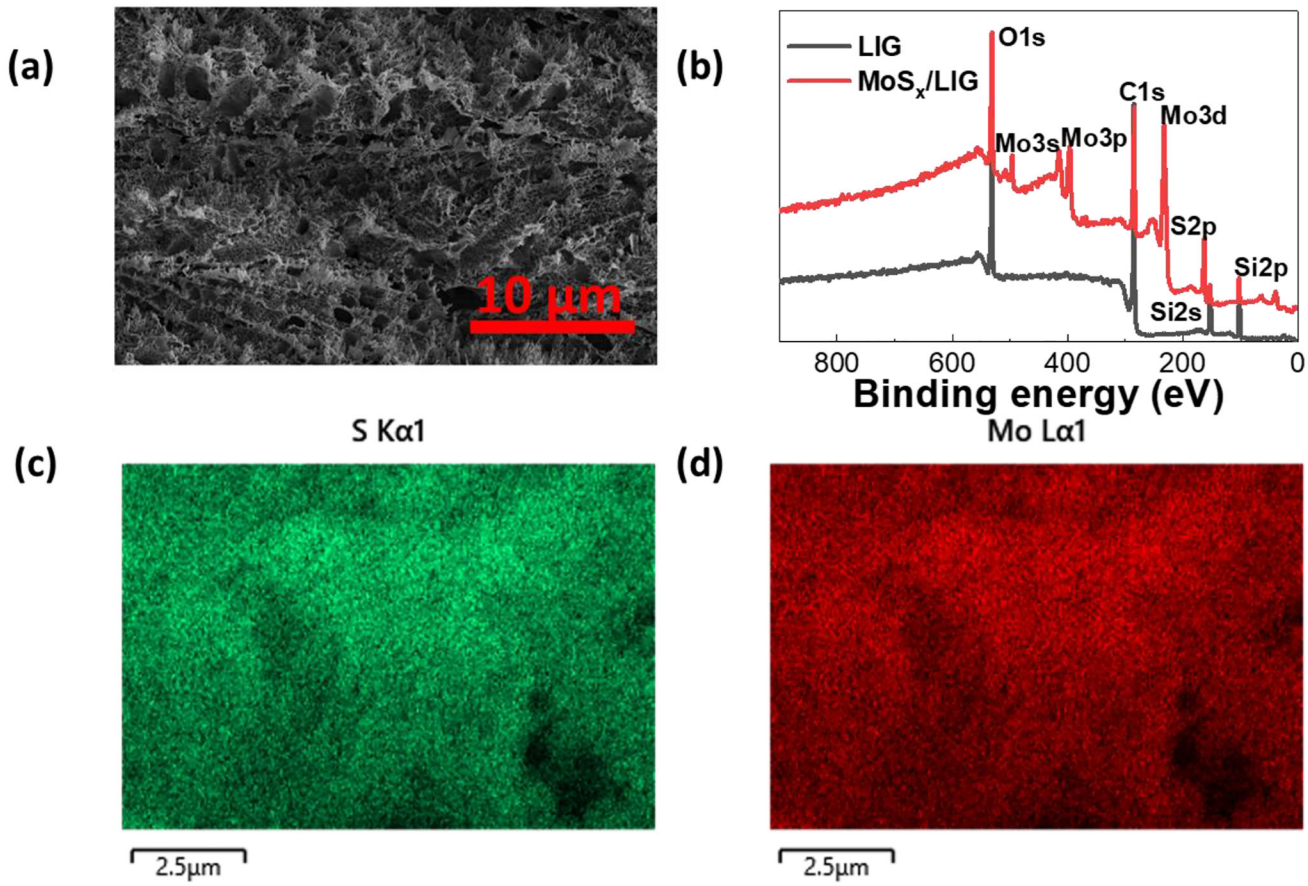

Figure 2.

(a) SEM image of the LIG and **(b)** XPS survey spectra of LIG and MoS_x/LIG showing its chemical components. EDS mapping of MoS_x/LIG shows the uniform presence **(c)** S and **(d)** Mo.

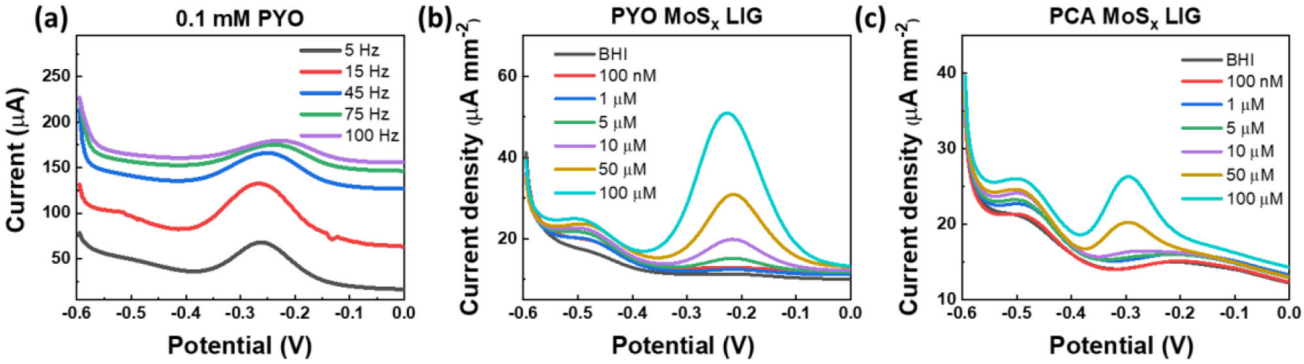

Figure 3.

(a) The Square wave voltammetry (SWV) curves of 1mM PYO at different frequencies. **(b)** The SWV curves of MoS_x/LIG with 0.1~100 uM PYO and **c)** PCA in BHI. SWV is performed from −0.6 to 0 V at a frequency of 15 Hz and an amplitude voltage of 50 mV.

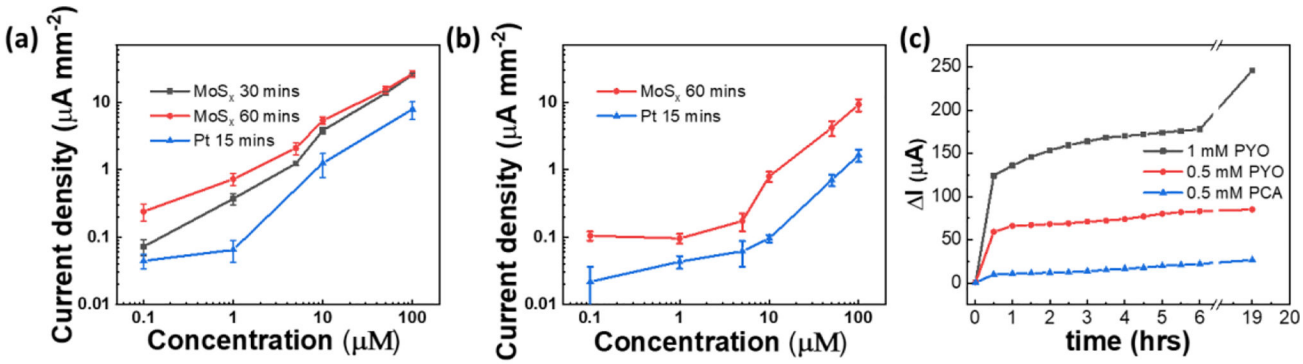

Figure 4.

The calibration curve for **(a)** MoS_x/LIG (deposited at two different conditions: 30 min and 60 min) and Pt/LIG with PYO and **(b)** PCA in BHI. Three sensors were tested and the standard deviation is plotted as error bar. **(c)** Diffusion test results by depositing PYO or PCA on agar, followed by time-resolved SWV measurement. ΔI at different time points is calculated by subtracting the current at 0 hr.

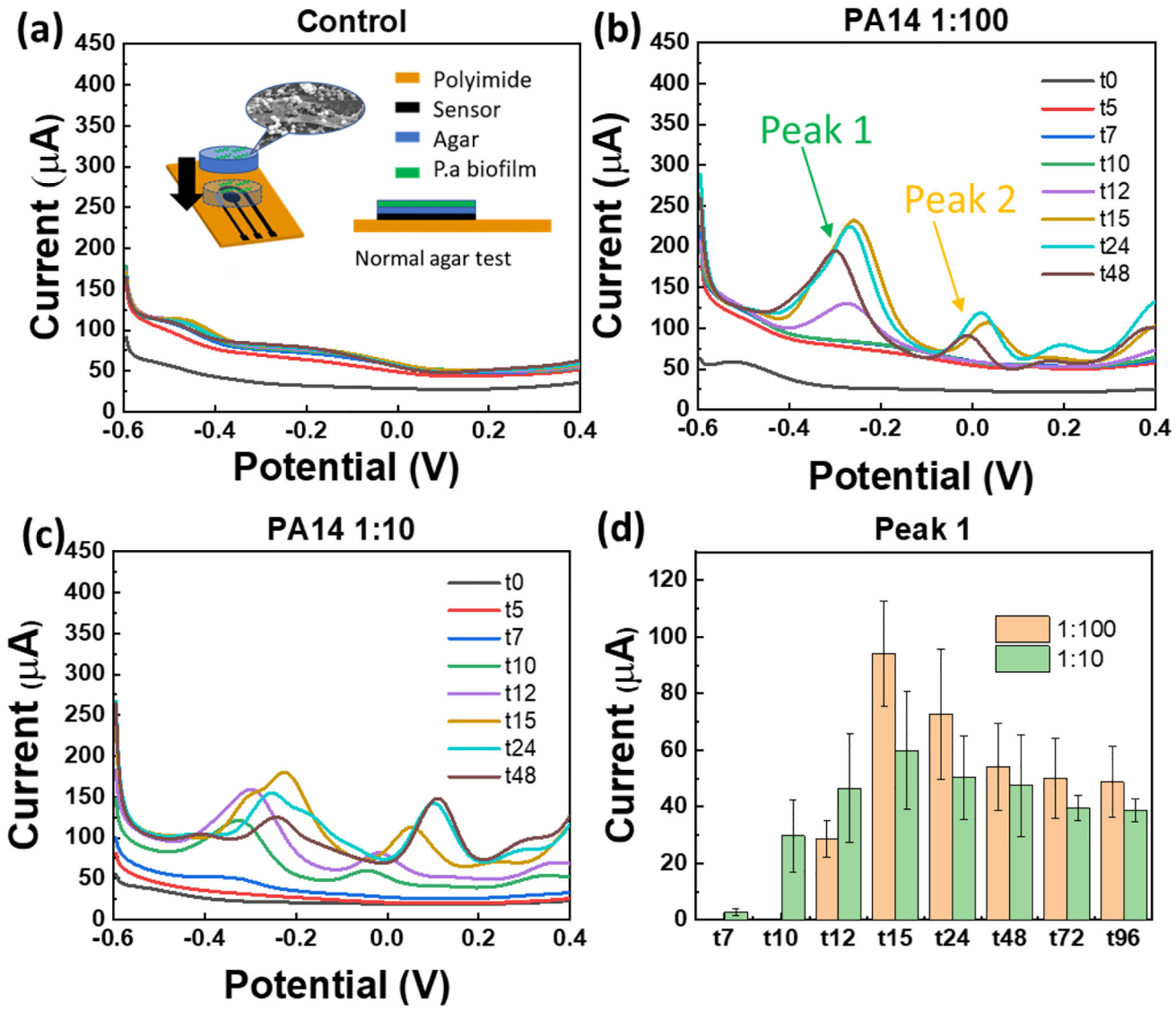

Figure 5.

SWV curves of the agar test with **(a)** *E. coli* (as negative control), **(b)** PA14 at seeding cell number of 1.4×10^5 CFU deposited over agar (diameter 6 mm). Arrows indicate two dominant peaks in time-dependent tests with biofilms, **(c)** Effect of seeding density was studied by depositing 1.4×10^6 CFU PA14 cells on agar (same dimensions as part b). **(d)** The current of peak 1 at about – 0.25 V (PYO and PCA peak) extracted from the data in plots b and c. Inset of part a shows schematic of the "normal agar test", i.e. when cells are not in direct contact with sensor.

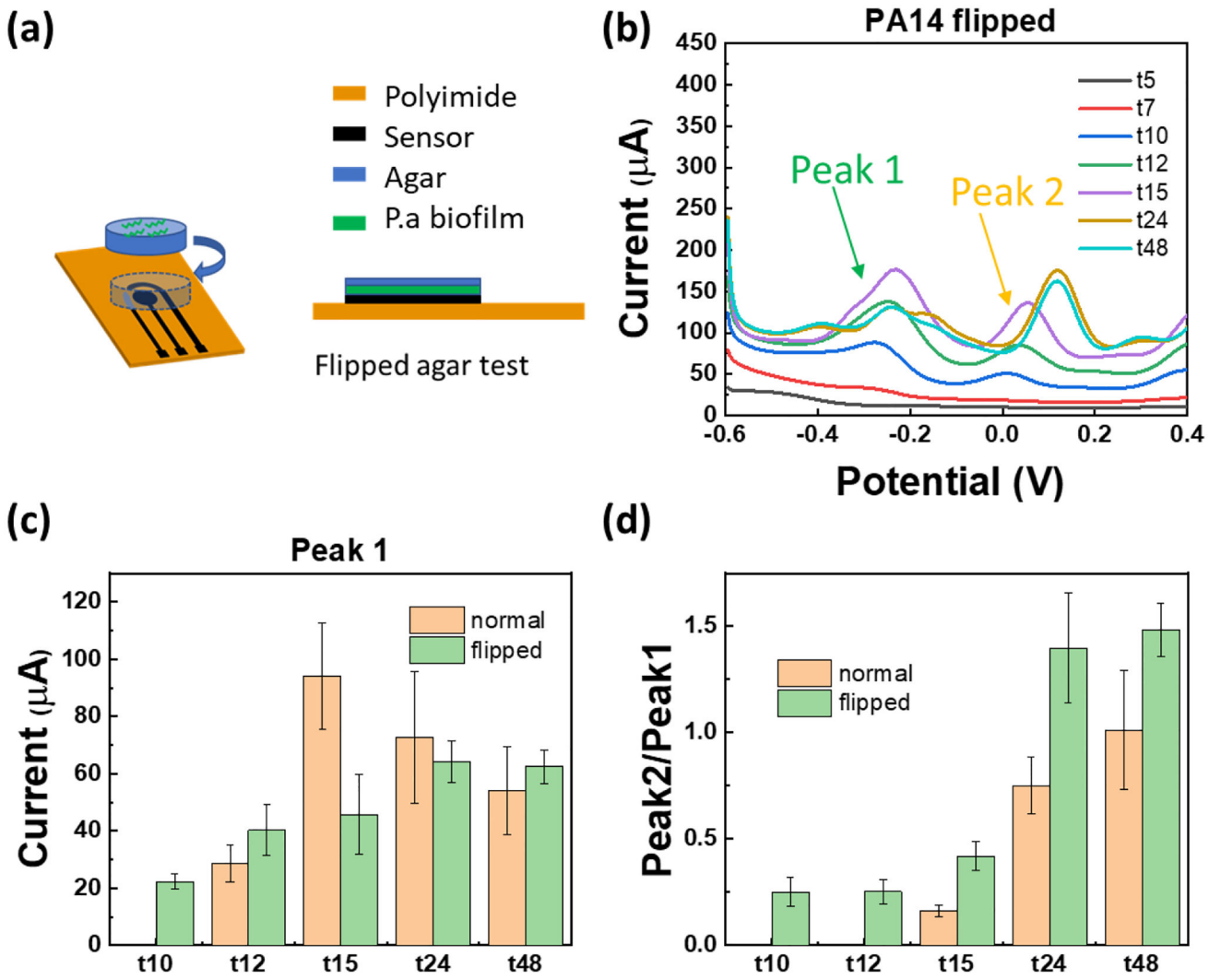

Figure 6.

(a) Schematic of the "Flipped agar test", i.e. when cells are in direct contact with the sensor. **(b)** SWV of flipped agar test with PA14 (seeded at initial cell number of 1.4×10^5 CFU over agar). **(c)** Comparison of the two test configurations in this study ("Normal" vs "Flipped"). The current of peak 1 at about – 0.25 V is plotted which corresponds to PYO and PCA (they usually overlap in PA biofilms). **(d)** The ratio of SWV current at peak 1 and peak 2 (shown by arrow in part b) as a function of time with two testing configurations is plotted, showing that the phenazines synthesis/interplay varies with time. The peak ratio from each SWV curve is calculated individually and the average and standard error are plotted. "Normal" includes data from three sensors (two SWV scans from each sensor) and for "Flipped" configuration, data from four sensors is included (two SWV scans from each sensor).

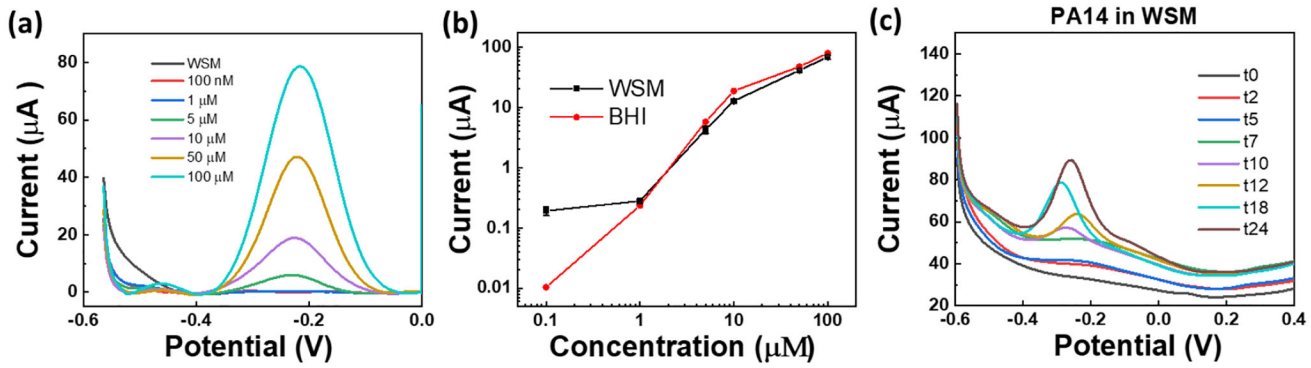

Figure 7.

(a) The SWV curves of MoS_x/LIG with 0.1~100 uM PYO spiked in WSM. **(b)** Calibration curves obtained from the SWV data. **(c)** SWV of PA14 in WSM monitored over time. SWV was performed using a potential step of 5 mV and an amplitude of 50 mV at 15 Hz.

Table 1.

Comparison of this work with other electrochemical methods.

Material	Fabrication Method	Technique	Test medium	LOD of PYO [μM]	Linear Range [μM]	Ref
Carbon	Screen printed	SWV	TSB	0.038	0–100	3
Carbon	Screen printed	SWV	LB, urine, bronchial lavages, sputum and heparinized blood	0.13 in sputum 0.18 in LB	1–100	4
Transparent carbon with chitosan gold nanoparticles	Lithography	SWV	LB with sodium phosphate buffer	1.6	1–100	20
Transparent carbon ultramicroelectrode arrays	Lithography	SWV CV	TSB and LB	1.0 ± 0.3	1–250	22
Nanopore electrode arrays	Nano fabrication	SWV CV With redox cycling	Fastidious Anaerobe Broth	0.01	1–100	23
Carbon nanotubes	Ink-jet printed	SWV	Wound simulating medium	0.1	0.1–100	24
Carbon	Screen printed	SWV	Agar-Au/Ag nanoalloy with human serum, whole blood, saliva	0.04	0.12–25	25
PANI/Au NPs	Electrochemical deposition	CV	LB	0.5	1.9–238	27
Gold coated nanograss	Deep reactive ion etching and ebeam deposition	SWV CV	Hypertonic saline and airway samples from cystic fibrosis patients	0.172	0.3125–25	28
Gold	Screen printed	CV	Mixture of pyoverdine, NAD, NADH, NADP, NADPH, phenazine, and LB and human saliva	2	2–100	29
Gold coated with a catechol-chitosan film	Electrodeposition and grafting redox-active catechols onto a chitosan film	DPV	LB	0.05	0.05–40	66
Carbon	Pad printed	SWV	Britton–Robinson buffer, Simulated wound fluid, Human serum	0.15	0.336–10	67
Carbon	Printed on glove	SWV	Hydrogel	3.33×10^{-3}	0.01–0.1	68
Carbon fiber	Laminated carbon fibre tow	SWV	Britton–Robinson buffer and P. aeruginosa broth	0.03	1–100	69
LIG	Direct laser printing and electrochemical deposition	SWV	Brain Heart Infusion Cetrimide agar Wound simulating medium	0.19	1–100	**This work**

Abbreviations: LOD—limit of detection, CV—cyclic voltammetry, SWV—square wave voltammetry, DPV—differential pulse voltammetry, LB—Lysogeny Broth, TSB— Tryptic Soy Broth